

Wavepacket Self-Rotation and Helical Zitterbewegung in Symmetry-Broken Honeycomb Lattices

Xiuying Liu, Frane Lunić, Daohong Song,* Zhixuan Dai, Shiqi Xia, Liqin Tang, Jingjun Xu, Zhigang Chen,* and Hrvoje Buljan*

The toolbox quantities used for manipulating the flow of light include typically amplitude, phase, and polarization. Pseudospins, such as those arising from valley degrees of freedom in photonic structures, have recently emerged as an excellent candidate for this toolbox, in parallel with rapid development of spintronics and valleytronics in condensed-matter physics. Here, by employing symmetry-broken honeycomb photonic lattices, valley-dependent wavepacket self-rotation manifested in spiraling intensity patterns is demonstrated, which occurs without any initial orbital angular momentum. Theoretically, it is shown that such wavepacket self-rotation is induced by the Berry phase and results in Zitterbewegung oscillations. The frequency of Zitterbewegung is proportional to the gap size, while the helicity of self-rotation is valley-dependent, i.e., correlated with the Berry curvature. These results lead to new understanding of the venerable Zitterbewegung phenomenon from the perspective of topology and are readily applicable on other platforms such as 2D Dirac materials and ultracold atoms.

have reshaped the traditional perspective, leading to the development of spintronics^[1] and valleytronics.^[2] Amplitude, phase, and polarization are the key quantities of usual recipes for controlling the flow of light. However, the understanding and development of optical spin–orbit interactions,^[3] photonic pseudospins,^[4] and valley degrees of freedom^[5–12] have offered us new knobs that can be used for manipulation of light in photonic structures, in analogy with parallel advances in electric systems.

The pioneering achievements exploiting valley degrees of freedom in photonics include, e.g., the prediction^[5,6] and experimental demonstration^[8] of photonic valley-Hall topological insulators, topologically protected refraction of robust kink states in valley photonic crystals,^[7] topological valley-Hall edge

states,^[9] and spin and valley-polarized one-way Klein tunneling.^[11] Photonic valley systems can be implemented at telecommunication and terahertz wavelengths on a silicon platform,^[12,13] at subwavelength scales on plasmonic platforms,^[8,14,15] and they can be used for the development of topological lasers,^[16–19] which opens the possibilities for many applications. Besides electromagnetic waves, valley topological materials have been used for manipulation of other waves such as sound waves^[20] and elastic waves.^[21] All these exemplary successes unequivocally point at the need and importance of discovering valley-dependent wave phenomena, for both fundamental understanding and advanced applications.

To this end, it is important to understand the behavior of physical quantities that distinguish different valleys. Among the most studied examples in photonics are the two inequivalent valleys of the honeycomb lattices (HCLs), located at the lattice high-symmetry K and K' points in the Brillouin zone, which are furnished with the nontrivial Berry phase winding.^[22,23] The Berry curvatures are in opposite directions at K - and K' -valleys in a (symmetry-broken) HCL (e.g., see ref. [23]), and thus can be used to distinguish the two valleys. Besides the Berry curvature, in electronic systems, the electron magnetic moment can also be used to distinguish the two valleys.^[24,25] The magnetic moment occurs from the self-rotating electric wavepacket,^[24–26] which is virtually impossible to be directly observed with electrons.


Here, we study valley-dependent propagation of light in an inversion-symmetry-broken photonic HCL. We establish the

1. Introduction

Electric charge is the key quantity for controlling signals in conventional electronics and semiconductor devices. However, advances in manipulating spin and valley degrees of freedom

X. Liu, Prof. D. Song, Z. Dai, S. Xia, Prof. L. Tang, Prof. J. Xu, Prof. Z. Chen, Prof. H. Buljan
The MOE Key Laboratory of Weak-Light Nonlinear Photonics
TEDA Applied Physics Institute and School of Physics
Nankai University
Tianjin 300457, China
E-mail: songdaohong@nankai.edu.cn; zgchen@nankai.edu.cn; hbuljan@phy.hr

F. Lunić, Prof. H. Buljan
Department of Physics
Faculty of Science
University of Zagreb
Bijenička cesta 32, Zagreb 10000, Croatia
Prof. D. Song, Prof. J. Xu, Prof. Z. Chen
Collaborative Innovation Center of Extreme Optics
Shanxi University
Taiyuan Shanxi 030006, P. R. China
Prof. Z. Chen
Department of Physics and Astronomy
San Francisco State University
San Francisco, CA 94132, USA

 The ORCID identification number(s) for the author(s) of this article can be found under <https://doi.org/10.1002/lpor.202000563>

DOI: 10.1002/lpor.202000563

lattice by employing a direct laser-writing technique,^[27] and we demonstrate experimentally and numerically the valley-dependent helicity in spiraling intensity patterns related to wavepacket self-rotation. Specifically, we show that, by selective excitation of the valleys in a gapped HCL, a probe beam undergoes distinct spiraling during propagation through the lattice, characterized by its helical intensity pattern and “center-of-mass” oscillation, even though no initial orbital angular momentum is involved. We theoretically demonstrate that the observed phenomenon dwells upon the existence of the Berry phase,^[28] leading to the fundamental phenomenon of Zitterbewegung, first introduced by Schrödinger^[29] in the context of relativistic electrons. We find that the helicity of Zitterbewegung in our system is a valley-dependent quantity.

Zitterbewegung refers to a prediction that elementary particles such as electrons described by the relativistic Dirac equation would exhibit rapid oscillatory motion in vacuum, with angular frequency on the order of $2mc^2/\hbar$.^[29] It was studied in attempts to provide a deeper understanding of the electron spin^[30,31] and even to interpret some aspects of quantum mechanics,^[32] but the Zitterbewegung of electrons in vacuum has never been observed owing to its inherent ultra-small amplitude and ultra-high frequency. However, electrons in Bloch bands of some materials are driven by equations analogous to the relativistic Dirac equation, e.g., Zitterbewegung of electrons was predicted to occur in semiconductor quantum wells.^[33] In a full analogy, Zitterbewegung was also predicted with ultracold atoms in optical lattices^[34] and with photons in 2D photonic crystals.^[35] Experimental observation of Zitterbewegung-like phenomena was, however, mostly limited to 1D domain in systems including trapped ions,^[36] photonic lattices,^[37] and Bose–Einstein condensates,^[38,39] or to surface acoustic waves in an integrated phononic graphene.^[40] The Zitterbewegung term in the quantum expectation value of the position operator vanishes if the wave-packets are made up with solely positive (or negative) energy states, thus leading to its interpretation in terms of interference of positive and negative energy states. In periodic lattices, this amounts to the interference of Bloch waves from different bands. In this work, we show theoretically that the Zitterbewegung can be interpreted via interference between the incident nonvortex beam component and the vortex component arising from the universal momentum-to-real space mapping mechanism, which inherently has a topological origin.^[41] Thus, we provide a different perspective about the Zitterbewegung phenomenon, which gives rise to a simpler visualization than the original interpretation.

2. Results

2.1. Experimental Results and Numerical Simulations

We study light propagation in (2+1)D photonic lattices, which in the paraxial approximation is governed by the Schrödinger-like equation (e.g., see ref. [23] and references therein)

$$i \frac{\partial \Psi}{\partial z} = -\frac{1}{2k_0} \nabla^2 \Psi - \frac{k_0 \delta n(x, y)}{n_0} \Psi(x, y, z) \quad (1)$$

here $\Psi(x, y, z)$ is the complex amplitude of the electric field, k_0 is the wave number in the medium, n_0 is the background refrac-

tive index, and $\delta n(x, y)$ is the induced refractive-index changes forming the HCL with broken inversion-symmetry, as illustrated in Figure 1a. Equation (1) is mathematically equivalent to the Schrödinger equation describing electrons in 2D quantum systems, with z playing the role of time. The HCL is comprised of two sublattices (**A** and **B**), and the inversion-symmetry breaking is achieved with a refraction index offset between the sublattices, see Figure 1a. In k -space, the HCL has two distinct valleys located at the K and K' points in the Brillouin zone (they are also referred to as Dirac points), as illustrated in Figure 1b. In the vicinity of Dirac points, the band structure is described by $\pm\sqrt{k^2 + m^2}$ (k is the magnitude of the wavevector with origin at the Dirac point, and m is the effective mass determined by band dispersion), and the wave dynamics is approximately described by the 2D massive Dirac equation (see theoretical analysis below). The size of the band gap is $2m$, and it is proportional to the refraction index offset between the two sublattices, as illustrated in Figure 1c for the photonic lattices used in our numerical simulations and experiments. For direct comparison, the insets in Figure 1c show the band structure close to the K -point for $m = 0$ (gapless Dirac-cone type band structure), and for $m > 0$ (gapped $\pm\sqrt{k^2 + m^2}$ type band structure).

Our main finding is sketched in Figure 1b. The probe beam which is formed by interfering three broad Gaussian beams excites the modes in the vicinity of three equivalent K -points (or K' -points) in momentum space, i.e., the modes in one valley, with both sublattices equally excited in real space. The output beam exhibits self-rotation during propagation through the HCL, which has a spiraling intensity pattern with the helicity depending on the valley (K or K') that is initially excited. It will be shown below that this spiraling self-rotating motion is attributed to a root of the Zitterbewegung of the wavepacket, identified through the rotation of its “center-of-mass” (COM), which is defined as the space average value $\langle \mathbf{r} \rangle = \int \mathbf{r} I(\mathbf{r}) d\mathbf{a}$ weighted with respect to intensity $I(\mathbf{r})$.

In Figure 1d–f, we show numerical results of the output patterns of the probe beam at different propagation distances in the inversion-symmetry-broken HCL, obtained by solving Equation (1), with the refractive index offset between the sublattices set by the ratio $n_A : n_B = 1.2:1$, exciting only the K valley. The parameters used in the simulations correspond to that of the experiment: $n_0 = 2.35$ for the SBN:61 crystal, $k_0 = 2\pi n_0/\lambda$ and $\lambda = 488$ nm, the lattice constant is $16 \mu\text{m}$ (i.e., the distance between nearest neighboring sites is $9 \mu\text{m}$), and the maximal index change (depth of the lattice) is about 1.3×10^{-4} . The overall envelope of the probe beam is Gaussian-like (Figure 1d), but with a triangular lattice structure (due to three-beam interference) at $z = 0$ that can be positioned to excite one or both sublattices. In simulations displayed in Figure 1d–f, the probe beam excites the middle points between the **A** and **B** sublattices, i.e., both sublattices are equally excited. We find that the output wavepacket exhibits self-rotation during propagation (see the Video in Supporting Information), and the initially symmetric probe beam evolves into an asymmetric spiraling intensity pattern as displayed in Figure 1e,f. It expands during propagation because of diffraction, whereas the spiral helicity and the direction of rotation are valley-dependent. In Figure 1g, the dynamical evolution of the beam’s COM is plotted in 3D, showing spiral-like Zitterbewegung oscillations (in the

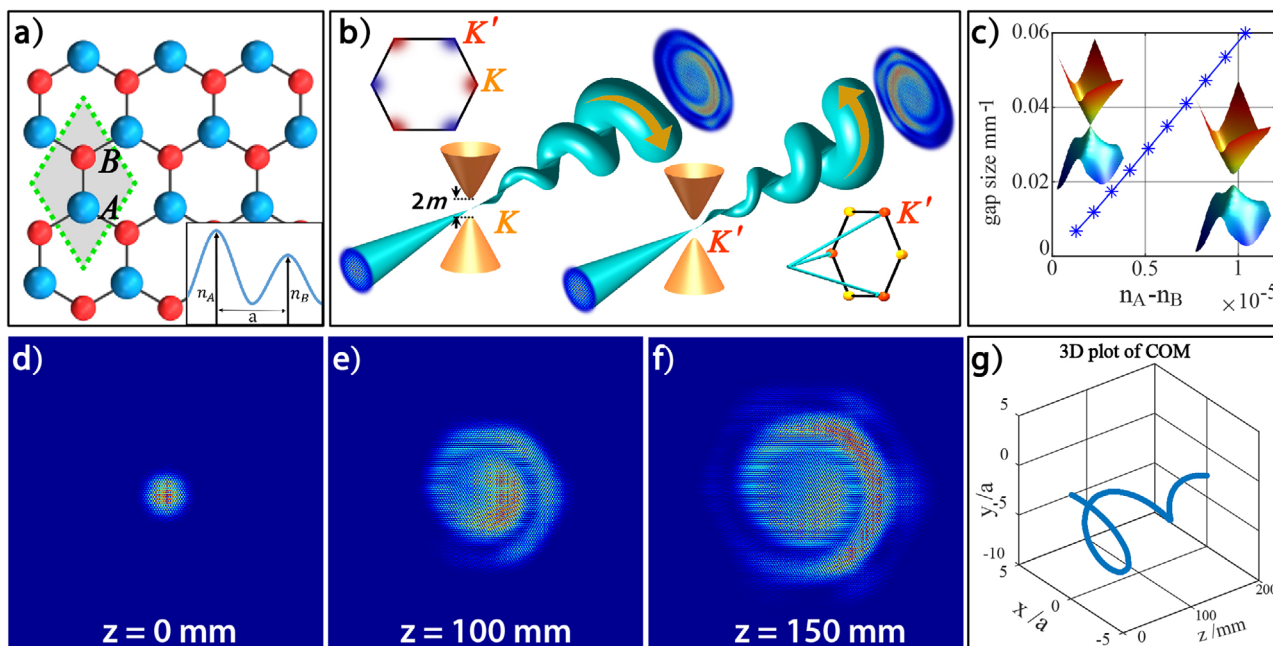


Figure 1. Valley-dependent wavepacket self-rotation in a symmetry-broken HCL. a) Illustration of an inversion-symmetry-broken HCL consisting of **A** and **B** sublattices. The inset sketches the refractive-index offset ($n_A > n_B$ is shown, e.g.). b) Illustration of wavepacket self-rotation when the modes in the vicinity of the K -valley (or K' -valley) are excited, showing spiraling intensity patterns with valley-dependent helicity. Top inset shows the valley locations at the edges of the first Brillouin zone in k -space; the Berry curvature is opposite at two inequivalent valleys (sketched with red and blue colors). Bottom inset shows the scheme when three K -valleys are simultaneously excited. c) The size of the gap as a function of the index offset ($n_A - n_B$) for photonic lattices used in our experiments. The insets show the band-gap structures in the vicinity of the K -point for $n_A - n_B = 0$ (upper inset), and $n_A - n_B > 0$ (lower inset). d–f) Spiraling intensity patterns at different propagation distances indicating self-rotation of the wavepacket. g) Plot of the COM trajectory obtained numerically. The probe at $z = 0$ shown in (d) has a Gaussian envelope with no initial orbital angular momentum—see video file in the Supporting Information.

plot we subtracted the drift which standardly occurs alongside Zitterbewegung phenomenon for better visualization).

Next, we present corresponding experimental results obtained in an HCL established in a 20 mm long nonlinear crystal by a cw-laser-writing method.^[27] Instead of using a single Gaussian beam for writing, here the two sublattices are separately written and controlled by a triangular lattice pattern. The refractive-index difference of the two sublattices $n_A : n_B$ is readily tuned by the writing time for each sublattice (see the Experimental Section). A typical example of experimentally generated symmetry-broken HCL with $n_A > n_B$ is shown in **Figure 2a**. As in simulation, the probe beam is a truncated triangular lattice pattern formed by interfering three broad Gaussian beams (see **Figure 2b**) with their wavevectors matched to the three K - or K' -points. In real space, we excite both sublattices with equal amplitude and phase by positioning the probe beam at middle points between the two sublattices. The observed intensity patterns of the probe beam at the lattice output under different excitation conditions are shown in the top panels of **Figure 2c–f**, with corresponding numerical simulation results plotted in the bottom panels.

When the input beam excites the K -valley with the refractive-index offset between sublattices such that $n_A > n_B$, the beam evolves into a spiraling pattern (**Figure 2c**). The helicity of the spiraling pattern and therefore the rotation direction of the output beam is reversed if the offset is changed to be $n_A < n_B$

(**Figure 2d**). As we will show theoretically below, such spiraling intensity pattern is related to the circular motion of the COM of the wavepacket and the Berry-phase-mediated Zitterbewegung. We emphasize that the rotation can only be realized when the inversion symmetry of the HCL is broken and the gap opens; for comparison, when $n_A = n_B$, the output pattern exhibits conical diffraction^[42] rather than a spiraling pattern (**Figure 2e**) under the equal excitation condition. Importantly, we experimentally demonstrate that the rotation direction depends on the valley degree of freedom. If we excite the K' valley instead of the K valley, while keeping all other conditions unchanged, we observe that the spiraling direction (i.e., helicity) of the intensity pattern is reversed; this can be seen by comparing the experimental results shown in **Figure 2c,f**. These observations are corroborated by numerical beam propagation simulations using Equation (1), which is shown in the bottom panels of **Figure 2**. We point out that altering the helicity of the spiraling pattern by reversing the index offset between the two sublattices (**Figure 2c** vs **Figure 2d**) is fully equivalent to altering the helicity via exciting different valleys (**Figure 2c** vs **Figure 2f**). In both cases, the helicity of the spiraling pattern is correlated with the direction of the Berry curvature around the gapped Dirac cone. In other words, the spiraling intensity is a valley contrasting quantity, analogous to the orbital momentum of electrons in condensed matter systems,^[24–26] manifested when the inversion symmetry is broken.

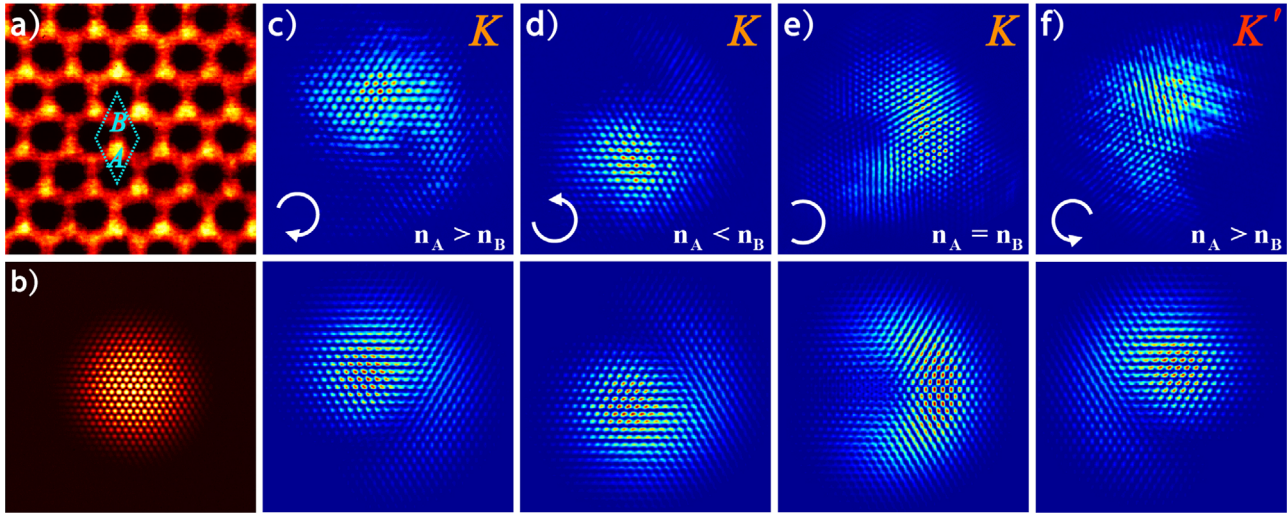


Figure 2. Experimental and numerical results demonstrating valley-dependent wavepacket self-rotation. a) Zoom-in image of a laser-written HCL with broken-inversion-symmetry; in this plot, $n_A > n_B$, corresponding to Figure 1a. b) Input triangular lattice pattern used in experiment as the probe beam. c–f) Experimental (top row) and numerical (bottom row) results of output intensity patterns for different excitation conditions: c–e) Results obtained under K -valley excitation where the index ratio is c) $n_A : n_B = 1.2:1$, d) $n_A : n_B = 1:1.2$, and e) $n_A : n_B = 1:1$. f) Result obtained under K' -valley excitation with $n_A : n_B = 1.2:1$. Note that the helicities of the spiraling patterns in (c) and (f) (as well as in (c) and (d)) are in opposite directions, as illustrated by curved arrows.

2.2. Theoretical Analysis

For excitations in the vicinity of the K -valley, Equation (1) is approximated by $i \frac{\partial \psi}{\partial z} = H \psi$, where the Hamiltonian (in k -space) is an effective 2D massive Dirac equation

$$H = \kappa (\sigma_x k_x + \sigma_y k_y) + \sigma_z m = \begin{pmatrix} m & \kappa (k_x - i k_y) \\ \kappa (k_x + i k_y) & -m \end{pmatrix} \\ = \begin{pmatrix} m & \kappa k e^{-i\varphi_k} \\ \kappa k e^{i\varphi_k} & -m \end{pmatrix} \quad (2)$$

where σ_i are the Pauli matrices. The coefficient κ depends on the coupling strength between adjacent waveguides in the lattice (e.g., see ref. [25]). Without any loss of generality, we set $\kappa = 1$ in all analytical expressions, because they can be rescaled to any value of κ with the substitution $k \rightarrow \kappa k$. The complex amplitude

of the electric field $\psi = \begin{pmatrix} \psi_{\frac{1}{2}} \\ \psi_{-\frac{1}{2}} \end{pmatrix}$ is a two-component spinor, because the HCL has two sublattices. Pseudospin components $\psi_{\frac{1}{2}}$ and $\psi_{-\frac{1}{2}}$ describe the field amplitudes in the A and B sublattices (e.g., see ref. [41]). The eigenmodes of the Hamiltonian in Equation (2) are given by $H \psi_{nk} = \beta_{nk} \psi_{nk}$,

$$\psi_{nk} = \frac{1}{\sqrt{N_{nk}}} \begin{pmatrix} \frac{m + \beta_{nk}}{k} e^{-i\varphi_k} \\ 1 \end{pmatrix}, \quad N_{nk} = 2 + \frac{2m(m + \beta_{nk})}{k^2} \quad (3)$$

where $\beta_{nk} = n \sqrt{k^2 + m^2}$; $n = \pm 1$ is the band number, and \mathbf{k} is the wavevector with origin at the K -point. It is important to note that the k -space topological charges of the two spinor components in Equation (3) differ by one, i.e., the vorticity of the two spinor components in k -space is different. This difference is indepen-

dent of the gauge used, and it gives rise to the Berry phase winding around the K -point.

Dynamics around the K' -valley is described analogously with substitution $k_x \rightarrow -k_x$ in Equation (2).^[25] The eigenmodes at the K' -valley are given by ψ_{nk}^* , i.e., the winding of the spinor vorticity in k -space is in the opposite direction. Thus, the geometry of the eigenmodes gives rise to the Berry curvature which is in opposite directions at the K and K' points^[23,25,26] (see Figure 1b). This is the origin of the opposite helicity of the spiraling patterns observed in Figure 2c,f.

We are interested in the dynamics from an axially symmetric initial excitation

$$\psi(r, \varphi_r, z = 0) = \psi_0 \sqrt{I_0(r)} = \int d^2k \psi_0 f(k) e^{ik \cdot r} \quad (4)$$

where we have introduced radial coordinates ($x = r \cos \varphi_r$ and $y = r \sin \varphi_r$), $f(k)$ corresponds to the spatial power spectrum of the initial excitation $f(k) = (2\pi)^{-2} \int \sqrt{I_0(r)} e^{-ik \cdot r} da$, and it determines the distribution of excitations around the K or K' -point;

$\psi_0 = \begin{pmatrix} \cos \theta e^{i\alpha} \\ \sin \theta \end{pmatrix}$ is the most general initial spinor, where α is the relative phase between the fields in the sublattices at $z = 0$, and θ determines the amplitude in each sublattice.

Dynamics from the initial condition (4) is readily found by expanding into eigenmodes of the system. After a straightforward calculation one finds

$$\psi(r, \varphi_r, z) = \begin{pmatrix} \psi_{\frac{1}{2}}(r, \varphi_r, z) \\ \psi_{-\frac{1}{2}}(r, \varphi_r, z) \end{pmatrix} = \begin{pmatrix} g_{\frac{1}{2},0}(r, z) + g_{\frac{1}{2},-1}(r, z) e^{-i\varphi_r} \\ g_{-\frac{1}{2},+1}(r, z) e^{i\varphi_r} + g_{-\frac{1}{2},0}(r, z) \end{pmatrix} \quad (5)$$

where $z = 13/\kappa k_0$, and the g -functions can be expressed as integrals in k -space (see the Supporting Information). In

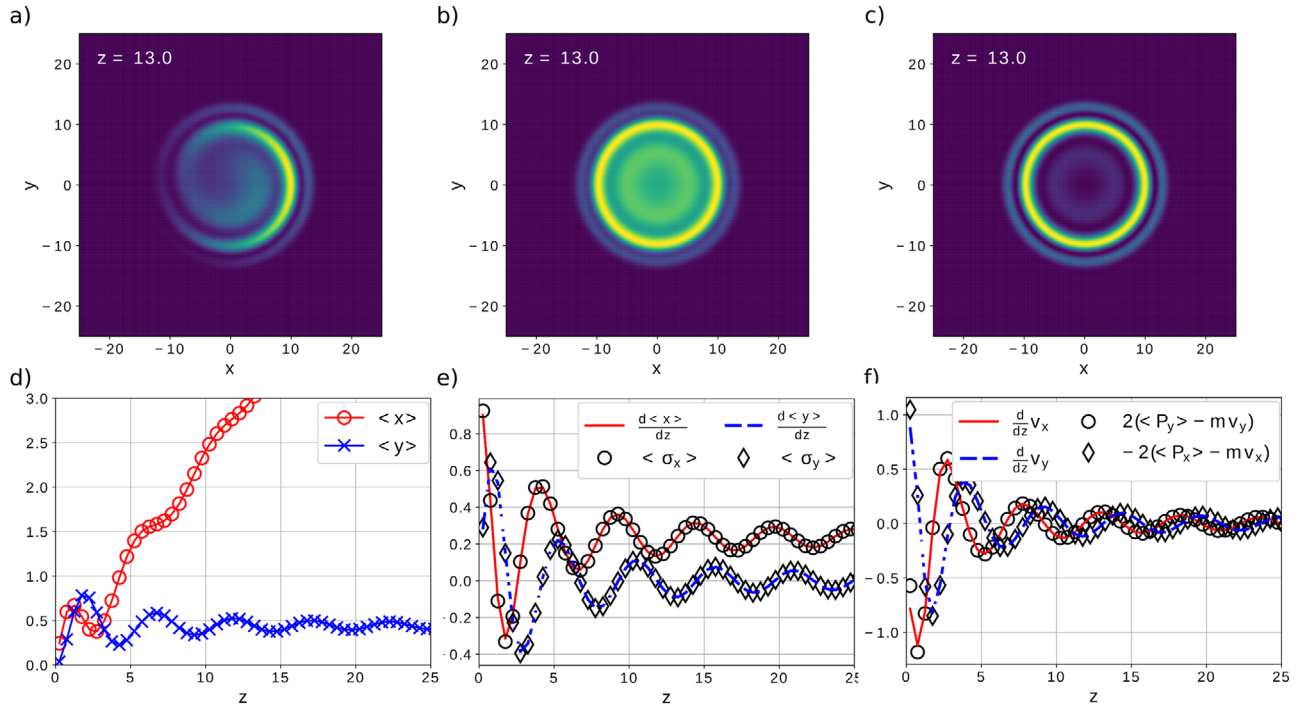


Figure 3. Theoretical analysis of wavepacket self-rotation from Dirac equation. Top panels are the spinor components of the intensity structure of the spiraling beam, and bottom panels show the motion of its “center-of-mass (COM).” In the figure, z is in units $(\kappa k_0)^{-1}$, x and y are in units k_0^{-1} . a) Intensity structure of the pseudospin component $|\psi_{\frac{1}{2}}^-(r, \varphi_r, z)|^2$, b) the nonvortex component $|g_{\frac{1}{2},0}^1(r, z)|^2$, and c) the vortex component $|g_{\frac{1}{2},-1}^1(r, z)|^2$. d) The position of the COM of the wavepacket (average values of x and y) as functions of z . e) Propagation of the velocity components of the COM, and the (identical) expectation values $\langle \sigma_x \rangle$ and $\langle \sigma_y \rangle$. f) Propagation of the acceleration components and numerical verification of Equation (10). See the text for details.

Figure 3a, we plot the spiraling intensity pattern $|\psi_{\frac{1}{2}}^-(r, \varphi_r, z)|^2$ obtained with the Hamiltonian in Equation (2); the envelope of the initial excitation is Gaussian, $f(k) = \exp(-k^2/k_0^2)$, and both sublattices are equally excited with same phase, $\psi_0 = \begin{pmatrix} 1 \\ 1 \end{pmatrix}$. The mass term is $m = 0.6\kappa k_0$, which determines the gap size. For our initial condition, the intensity in the lower spinor component $|\psi_{-\frac{1}{2}}^-(r, \varphi_r, z)|^2$ is equal to that in the upper component $|\psi_{\frac{1}{2}}^-(r, \varphi_r, z)|^2$, and consequently the whole intensity $|\psi|^2 = |\psi_{\frac{1}{2}}|^2 + |\psi_{-\frac{1}{2}}|^2$ has the same spatial dependence as $|\psi_{\frac{1}{2}}|^2$ illustrated in Figure 3a (see the Supporting Information). For this reason, in what follows we focus on understanding the intensity in just one spinor component. It is evident that the spiraling intensity pattern obtained with the “low-energy” Hamiltonian Equation (2) agrees with those obtained from numerical simulations of the Schrödinger Equation (1) as well as from experiments shown in Figure 2.

It is important to note from Equation (5) that each spinor component is a superposition of a nonvortex (Gaussian-like) amplitude and a vortex amplitude. At $z = 0$, there are no vortex components, because $g_{\frac{1}{2},-1}^1(r, 0) = g_{-\frac{1}{2},1}^1(r, 0) = 0$. The vortex components dynamically emerge during the propagation. The underlying mechanism behind the emergence of these vortices was explained previously:^[41] the vortex that is present in the k -space of each eigenmode of this system (related to inherent topological

singularity at the Dirac point) is mapped to the real space during linear propagation dynamics (analogous to the far-field mapping of the power spectra to real space intensity).

To explain the spiraling pattern observed in our experiments, we calculate the intensity in the pseudospin components

$$|\psi_{\frac{1}{2}}|^2 = |g_{\frac{1}{2},0}^1(r, z)|^2 + |g_{\frac{1}{2},-1}^1(r, z)|^2 + 2|g_{\frac{1}{2},0}^1||g_{\frac{1}{2},-1}^1| \cos(-\text{Arg } g_{\frac{1}{2},0}^1(r, z) + \text{Arg } g_{\frac{1}{2},-1}^1(r, z) - \varphi_r) \quad (6)$$

and equivalently for the other pseudospin component. The last term describes the interference between the vortex and nonvortex field amplitudes, which depends on their relative phase. The intensities of the nonvortex term $|g_{\frac{1}{2},0}^1(r, z)|^2$ and the vortex term $|g_{\frac{1}{2},-1}^1(r, z)|^2$ are radially symmetric, as shown in Figure 3b,c (see the Supporting Information for plots of all the g -functions). Therefore, the spiraling pattern must arise from the interference. The interference term has a maximum when

$$\varphi_r = -\text{Arg } g_{\frac{1}{2},0}^1(r, z) + \text{Arg } g_{\frac{1}{2},-1}^1(r, z) \text{ (modulo } 2\pi) \quad (7)$$

When $-\text{Arg } g_{\frac{1}{2},0}^1(r, z) + \text{Arg } g_{\frac{1}{2},-1}^1(r, z)$ is monotonically increasing (or decreasing) with r , the function implicitly given in Equation (7) is a spiral in the (r, φ_r) -plane; the spiral helicity depends on whether the r.h.s. in Equation (7) decreases or increases.

Evidently, the spiraling self-rotating pattern arises from the interference of the vortex and the nonvortex components.

We now present the theory for the wavepacket self-rotation and Zitterbewegung phenomenon in our system. Dynamics of the COM of the wavepacket $\mathbf{r}_C = x_C \hat{x} + y_C \hat{y}$ is given by

$$\mathbf{r}_C(z) = \langle \mathbf{r} \rangle = \int \psi^+ (r, \varphi_r, z) \mathbf{r} \psi (r, \varphi_r, z) da \quad (8)$$

where $\mathbf{r} = x\hat{x} + y\hat{y}$, and $da = r dr d\varphi_r$ is the infinitesimal area element. It can be understood by observing the velocity of the COM

$$\mathbf{v}_C = \frac{d\mathbf{r}_C}{dz} = \int \psi^+ (r, \varphi_r, z) i[H, \mathbf{r}] \psi (r, \varphi_r, z) da = \langle \sigma_x \rangle \hat{x} + \langle \sigma_y \rangle \hat{y} \quad (9)$$

and its acceleration

$$\frac{d\mathbf{v}_C}{dz} = -2\hat{z} \times \mathbf{P} + 2m\hat{z} \times \mathbf{v}_C \quad (10)$$

where we have introduced vector $\mathbf{P} = \langle k_x \sigma_z \rangle \hat{x} + \langle k_y \sigma_z \rangle \hat{y}$ (see the Supporting Information for the derivation). Calculated results from Equations (9) and (10) are illustrated in Figure 3d–f.

The second term in Equation (10) is the Zitterbewegung term; it corresponds to the oscillations of the COM with frequency $2m$ (the size of the spectral gap). Oscillations are clearly visible in all Figure 3d–f. Moreover, it is evident from Equation (10) that the helicity of Zitterbewegung oscillations depends on the sign of $m \propto n_A - n_B$, which corroborates our experimental findings. The first term in Equation (10) yields the drift of the COM of the wavepacket, visible in Figure 3d, which is an expected feature of the Zitterbewegung effect (e.g., see refs. [33,43]). The direction of the drift depends on the initial conditions. More specifically, the expectation value of the pseudospin operator $\sigma = \hat{x} \sigma_x + \hat{y} \sigma_y$ at $z = 0$ sets the direction of the initial velocity of the COM (see Figure 3e). Such drifting of the COM is also observed in our numerical simulations using Equation (1). We note that for better visualization of the spiraling dynamics, we did not include the drift when plotting Figure 1g.

The components of the vector \mathbf{P} are interpreted as the difference of the expectation value of the momentum between the pseudospin-up and -down components, i.e., the difference of the momentum between the two sublattices. The acceleration of the COM in the x -direction is proportional to P_y , which can be therefore interpreted as a pseudo-force exerted in the COM. From the example shown in Figure 3f, we see that this pseudo-force \mathbf{P} shows damped oscillations around zero. Thus, it induces some oscillations, which should be distinguished from those of the Zitterbewegung term. Our calculations indicate that the circular Zitterbewegung motion in symmetry-broken HCLs exists only when m is nonzero and thus the gap opens, which is in agreement with the Zitterbewegung of electrons.[29] Yet, our finding is in contradistinction with similar oscillations that were called Zitterbewegung in gapless HCL systems.[35,40,44] The oscillations reported there could be linked to the oscillations of the pseudo-force \mathbf{P} described above, rather than to the Zitterbewegung term which is absent for $m = 0$.

3. Discussion

The theory of the Zitterbewegung has been addressed in numerous papers.[30,32–35,45–47] The Zitterbewegung effect was originally associated with oscillatory motion of electrons in 3D space,[29,30] but such motion has never been observed. Here, we focus on the novel aspects of this phenomenon using optical wavepackets in 2D photonic lattices. We discuss connection between the experimentally observed valley-dependent spiraling intensity pattern (related to self-rotation of the wavepacket) and the Zitterbewegung phenomenon. This leads to a novel interpretation of the phenomenon, and sheds light on the role played by the Berry phase.

First, we mention a seemingly unrelated simple example. Considering two coupled single-mode waveguides, the coupled system has a symmetric and an antisymmetric eigenmode, $\frac{1}{\sqrt{2}}(u_L \pm u_R)$, with two propagation constants (eigenvalues) whose difference depends on the strength of the coupling (here the letter L stands for the left waveguide, and R for the right waveguide). By launching a beam, e.g., into the left waveguide, both modes will be excited and they will undergo beating; the field amplitude will thus jump from the left to the right waveguide and back and forth, with the frequency given by the coupling strength. The COM of the beam will oscillate at this frequency.

The very same mechanism, albeit a bit more complicated, leads to Zitterbewegung in our 2D system. First, we excite both sublattices of the HCL equally and with the same phase ($\psi_0 = \begin{pmatrix} \cos \theta e^{i\alpha} \\ \sin \theta \end{pmatrix} = \begin{pmatrix} 1 \\ 1 \end{pmatrix}$). The envelope of the initial excitation is Gaussian-like with azimuthal symmetry. In experiments and numerical simulations, the intensity fine structure under this envelope is a triangular lattice (it allows tuning the excitation of the two sublattices). In “low-energy” theory Equation (2), this means that the continuous field amplitudes $\psi_{\pm}(r, \varphi_r, z = 0)$ and $\psi_{\mp}(r, \varphi_r, z = 0)$ are independent of the azimuthal angle φ_r . Because of the nontrivial Berry phase winding around the Dirac points, i.e., the topology of the system, a vortex beam component (with φ_r dependent amplitude) will dynamically emerge. The underlying universal mechanism which maps the topological singularity (vortex) from the k -space to the real space was discovered recently.[41] As such, for $z > 0$, a single pseudospin component is furnished with both the nonvortex and the vortex beam components, which naturally interfere. It is demonstrated in the previous section and shown in Figure 3 that without the interference of these two components, the intensity pattern of the beam remains its azimuthal symmetry. The shape of the interference fringes depends on the evolution of the phase fronts of these two components, i.e., on $\text{Arg } g_{\frac{1}{2},0}(r, z) - \text{Arg } g_{\frac{1}{2},-1}(r, z)$, which yields a spiraling self-rotating pattern (see Figure 3). This rotation breaks the azimuthal symmetry of the initial beam and leads to oscillation of the COM of the beam $\mathbf{r}_C(z)$, in analogy to the two-mode beating discussed above. This alternative interpretation of the Zitterbewegung oscillations is perhaps more easily visualized than the original one invoking interference between positive and negative energy states. Both interpretations are correct, however, ours gives a simple picture for the circular oscillations of the COM associated with wavepacket self-rotation.

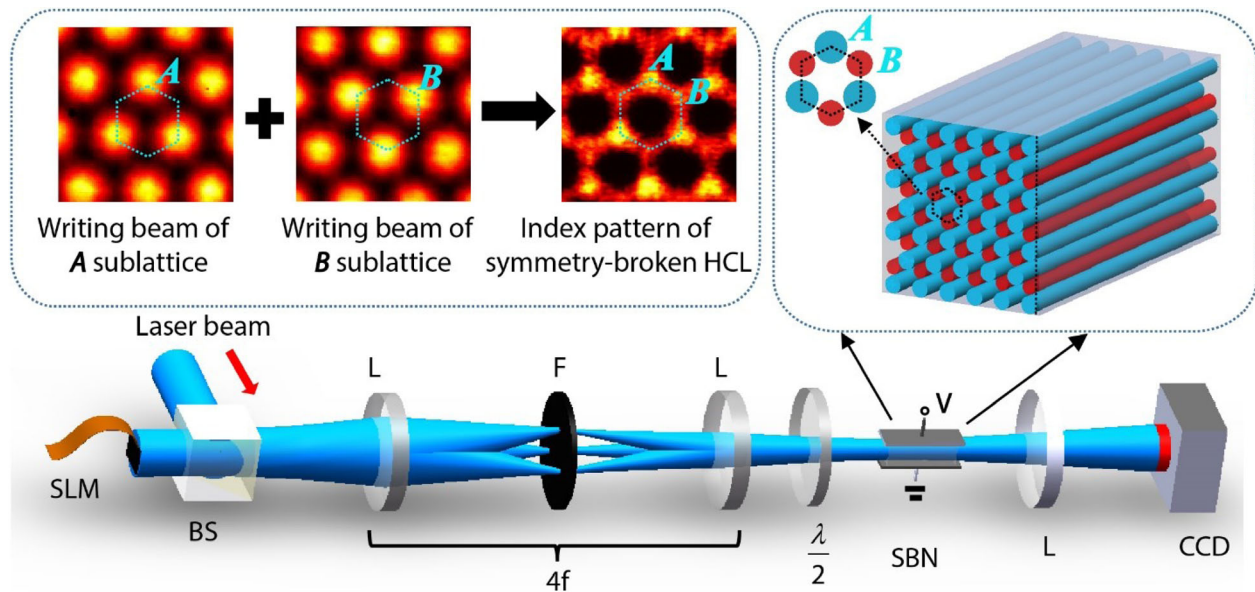


Figure 4. Experimental setup and scheme used for laser-writing the symmetry-broken HCL and for the observation of valley-dependent wavepacket self-rotation. SLM, spatial light modulator; BS, beam splitter; L, lens; F, Filter; $\frac{\lambda}{2}$, half-wave plate; SBN: strontium barium niobate crystal. The triangular lattice beam for alternatively writing the two sublattices and the superimposed lattice structure are shown in the top-left inset, and the 3D lattice structure through the crystal is illustrated in the top-right inset.

It should be emphasized that without the gap, there is no Zitterbewegung (see Equation (10)). This means that the gap is crucial for the existence of radial dependence of the phase fronts $\text{Arg } g_{\frac{1}{2},0}(r,z) - \text{Arg } g_{\frac{1}{2},-1}(r,z)$ that yields the spiraling intensity patterns. This can be understood because evolving phase fronts correspond to the dispersion curves. The dispersion curves drastically change when the gap opens, from the linear (conical) dispersion to the “parabolic” one. The helicity of the spiraling self-rotating motion determines the helicity of the Zitterbewegung of the COM. Consequently, it is valley-dependent in the symmetry-broken HCLs.

Let us digress a bit and comment on results of conical diffraction shown in Figure 2e, i.e., when $m = 0$ and the lattice band structure is a conical intersection. The far field intensity structure, i.e., the outcome of conical diffraction, depends on the initial excitation conditions, i.e., the weights and the relative phases of the Bloch modes excited around Dirac points. For example, if one excites both sublattices in phase, and simultaneously at both K - and K' -valleys, the output would be circularly symmetric.^[42] If one excites only a single sublattice at either K -valleys or K' -valleys, the output is also circularly symmetric.^[4] The crescent-like output in Figure 2e is a result when both sublattices are initially excited but at a single set (K or K') of valleys.

Finally, we discuss the crucial role played by the Berry phase. The existence of the Berry phase at each valley is responsible for the existence of the momentum to real space mapping which produces a vortex component in the field, even though that the initial excitation beam is Gaussian-like. The connection between the Berry phase and Zitterbewegung has been analyzed previously in literature.^[34] These analyses relied on the fact that the COM of the beam can be expressed as $\langle \mathbf{r} \rangle = \int \tilde{\psi}^+(\mathbf{k}, z) i \nabla_{\mathbf{k}} \tilde{\psi}(\mathbf{k}, z) d^2 k$ in the momentum space representation of the field amplitude.^[34,46] When $\tilde{\psi}(\mathbf{k}, z)$ is expressed in eigenmodes of the system, some

terms in the expression for $\langle \mathbf{r} \rangle$ will contain the Berry connection $\mathbf{A}_n(\mathbf{k}) = i \psi_{n\mathbf{k}}^+ \nabla_{\mathbf{k}} \psi_{n\mathbf{k}}$; however, the terms corresponding to Zitterbewegung will be nonzero only if the interband matrix elements $i \psi_{-1\mathbf{k}}^+ \nabla_{\mathbf{k}} \psi_{1\mathbf{k}}$ and $i \psi_{1\mathbf{k}}^+ \nabla_{\mathbf{k}} \psi_{-1\mathbf{k}}$ are nonzero (see the Supporting Information for the derivation). These matrix elements take very similar form to that of the Berry connection, except that the operator $i \nabla_{\mathbf{k}}$ is evaluated between modes of different bands. This is consistent with our experimental setting where both bands are excited. Thus, we conclude that in our observations, the key role of the Berry phase is to generate the vortex term enabling its interference with the nonvortex component, and hence the Zitterbewegung. The direction of the Berry curvature sets the helicity of the spiraling pattern, and therefore the valley-dependence of the spiraling self-rotating wavepacket.

4. Experimental Section

Experimental Setup and Scheme: In this experiment, the symmetry-broken HCL was established in a nonlinear photorefractive crystal (SBN:61; dimensions: $a \times b \times c = 5 \times 20 \times 5 \text{ mm}^3$) by using the cw-laser writing method established previously.^[27] Instead of using a single Gaussian beam for waveguide writing, here a triangular lattice beam formed by three-beam interference was employed. A collimated ordinarily polarized laser beam at a wavelength of 488 nm illuminated a spatial light modulator (SLM) loaded with a programmable phase mask, which was transformed into a triangular lattice pattern after passing through a 4f system combined with a filter. Such a lattice beam remained invariant through the 20 mm long crystal. The lattice-writing beam induced a triangular lattice due to the photorefractive self-focusing nonlinearity, as controlled by the beam power (4.8 mW), the bias electric field ($1.2 \times 10^5 \text{ V m}^{-1}$), and the writing time. The HCL could be established by alternatively writing the two sublattices, as illustrated in Figure 4, taking advantage of the “memory effect” of the photorefractive crystal. In addition, since the value of nonlinear refractive index change is proportional to the writing time, the

refractive index differences of the two sublattices could readily be tuned by using different writing time for each sublattice. As such, the same triangular lattice beam induced different index changes for different sublattices, leading to the desired inversion-symmetry-broken HCL as examined by a broad (quasi-plane-wave) beam (see the insets in Figure 4). To selectively excite the HCL, an extraordinarily polarized and truncated triangular lattice beam was sent into the lattice along the same optical path with the writing beam. However, the probe beam had a much smaller size that covered only several lattice sites, and its direction (with its three constituting components momentum-matched to three equivalent valleys) and launching position (for exciting both sublattices) could be precisely controlled by the SLM. To avoid the self-action of the probe beam due to nonlinearity, the intensity of the probe beam was set to be sufficiently low, so that it underwent linear propagation. The output intensity patterns of the probe beam through the lattice were recorded by a CCD camera.

Supporting Information

Supporting Information is available from the Wiley Online Library or from the author.

Acknowledgements

X.L. and F.L. contributed equally to this work. This research was supported by the National Key R&D Program of China under grant no. 2017YFA0303800, the National Natural Science Foundation (11922408, 91750204, 11674180), PCSIRT, and the 111 Project (no. B07013) in China. H.B. acknowledges support in part by the Croatian Science Foundation grant no. IP-2016-06-5885 SynthMagIA, and the QuantiX Lie Center of Excellence, a project co-financed by the Croatian Government and European Union through the European Regional Development Fund - the Competitiveness and Cohesion Operational Programme (Grant KK.01.1.1.01.0004).

Conflict of Interest

The authors declare no conflict of interest.

Data Availability Statement

Data sharing is not applicable to this article as no new data were created or analyzed in this study.

Keywords

Berry curvature, symmetry broken honeycomb lattice, valley degree of freedom, wavepacket self-rotation, Zitterbewegung

Received: December 10, 2020

Revised: March 9, 2021

Published online: May 26, 2021

- [1] J. F. Igor Žutić, S. Das Sarma, *Rev. Mod. Phys.* **2004**, 76, 323.
- [2] J. R. Schaibley, H. Yu, G. Clark, P. Rivera, J. S. Ross, K. L. Seyler, W. Yao, X. Xu, *Nat. Rev. Mater.* **2016**, 1, 16055.
- [3] K. Y. Bliokh, F. J. Rodríguez-Fortuño, F. Nori, A. V. Zayats, *Nat. Photonics* **2015**, 9, 796.

- [4] D. Song, V. Paltoglou, S. Liu, Y. Zhu, D. Gallardo, L. Tang, J. Xu, M. Ablowitz, N. K. Efremidis, Z. Chen, *Nat. Commun.* **2015**, 6, 6272.
- [5] T. Ma, G. Shvets, *New J. Phys.* **2016**, 18, 025012.
- [6] J. W. Dong, X. D. Chen, H. Zhu, Y. Wang, X. Zhang, *Nat. Mater.* **2017**, 16, 298.
- [7] F. Gao, H. Xue, Z. Yang, K. Lai, Y. Yu, X. Lin, Y. Chong, G. Shvets, B. Zhang, *Nat. Phys.* **2017**, 14, 140.
- [8] X. Wu, Y. Meng, J. Tian, Y. Huang, H. Xiang, D. Han, W. Wen, *Nat. Commun.* **2017**, 8, 1304.
- [9] J. Noh, S. Huang, K. P. Chen, M. C. Rechtsman, *Phys. Rev. Lett.* **2018**, 120, 063902.
- [10] X.-D. Chen, F.-L. Zhao, M. Chen, J.-W. Dong, *Phys. Rev. B* **2017**, 96, 020202.
- [11] X. Ni, D. Putseladze, D. A. Smirnova, A. Slobozhanyuk, A. B. Khanikaev, *Sci. Adv.* **2018**, 4, eaap8802.
- [12] M. I. Shalae, W. Walasik, A. Tsukernik, Y. Xu, N. M. Litchinitser, *Nat. Nanotechnol.* **2019**, 14, 31.
- [13] Y. Yang, T. Yamagami, X. Yu, P. Pitchappa, J. Webber, B. Zhang, M. Fujita, T. Nagatsuma, R. Singh, *Nat. Photonics* **2020**, 14, 446.
- [14] M. Jung, Z. Fan, G. Shvets, *Phys. Rev. Lett.* **2018**, 121, 086807.
- [15] M. Proctor, P. A. Huidobro, S. A. Maier, R. V. Craster, M. P. Makwana, *Nanophotonics* **2020**, 9, 657.
- [16] Y. Zeng, U. Chattopadhyay, B. Zhu, B. Qiang, J. Li, Y. Jin, L. Li, A. G. Davies, E. H. Linfield, B. Zhang, Y. Chong, Q. J. Wang, *Nature* **2020**, 578, 246.
- [17] H. Zhong, Y. Li, D. Song, Y. V. Kartashov, Y. Zhang, Y. Zhang, Z. Chen, *Laser Photonics Rev.* **2020**, 14, 2000001.
- [18] Y. Gong, S. Wong, A. J. Bennett, D. L. Huffaker, S. S. Oh, *ACS Photonics* **2020**, 7, 2089.
- [19] D. Smirnova, A. Tripathi, S. Kruk, M. S. Hwang, H. R. Kim, H. G. Park, Y. Kivshar, *Light: Sci. Appl.* **2020**, 9, 127.
- [20] J. Lu, C. Qiu, L. Ye, X. Fan, Z. Liu, *Nat. Phys.* **2017**, 13, 369.
- [21] M. Yan, J. Lu, F. Li, W. Deng, X. Huang, J. Ma, Z. Liu, *Nat. Mater.* **2018**, 17, 993.
- [22] L. Lu, J. D. Joannopoulos, M. Soljačić, *Nat. Photonics* **2014**, 8, 821.
- [23] T. Ozawa, H. M. Price, A. Amo, N. Goldman, M. Hafezi, L. Lu, M. C. Rechtsman, D. Schuster, J. Simon, O. Zilberberg, I. Carusotto, *Rev. Mod. Phys.* **2019**, 91, 015006.
- [24] D. Xiao, W. Yao, Q. Niu, *Phys. Rev. Lett.* **2007**, 99, 236809.
- [25] X. Xu, W. Yao, D. Xiao, T. F. Heinz, *Nat. Phys.* **2014**, 10, 343.
- [26] D. Xiao, M.-C. Chang, Q. Niu, *Rev. Mod. Phys.* **2010**, 82, 1959.
- [27] S. Xia, A. Ramachandran, S. Xia, D. Li, X. Liu, L. Tang, Y. Hu, D. Song, J. Xu, D. Leykam, S. Flach, Z. Chen, *Phys. Rev. Lett.* **2018**, 121, 263902.
- [28] M. V. Berry, *Proc. R. Soc. London, Ser. A* **1984**, 392, 45.
- [29] E. Schrödinger, *Sitzungsber. Preuss. Akad. Wiss., Phys.-Math. Kl.* **1930**, 24, 418.
- [30] K. Huang, *Am. J. Phys.* **1952**, 20, 479.
- [31] C.-P. Chuu, M.-C. Chang, Q. Niu, *Solid State Commun.* **2010**, 150, 533.
- [32] D. Hestenes, *Found. Phys.* **1990**, 20, 1213.
- [33] J. Schliemann, D. Loss, R. M. Westervelt, *Phys. Rev. Lett.* **2005**, 94, 206801.
- [34] J. Y. Vaishnav, C. W. Clark, *Phys. Rev. Lett.* **2008**, 100, 153002.
- [35] X. Zhang, *Phys. Rev. Lett.* **2008**, 100, 113903.
- [36] R. Gerritsma, G. Kirchmair, F. Zahringer, E. Solano, R. Blatt, C. F. Roos, *Nature* **2010**, 463, 68.
- [37] F. Dreisow, M. Heinrich, R. Keil, A. Tunnermann, S. Nolte, S. Longhi, A. Szameit, *Phys. Rev. Lett.* **2010**, 105, 143902.
- [38] L. J. Leblanc, M. C. Beeler, K. Jiménez-García, A. R. Perry, S. Sugawa, R. A. Williams, I. B. Spielman, *New J. Phys.* **2013**, 15, 073011.
- [39] C. Qu, C. Hamner, M. Gong, C. Zhang, P. Engels, *Phys. Rev. A* **2013**, 88, 021604(R).
- [40] S. Y. Yu, X. C. Sun, X. Ni, Q. Wang, X. J. Yan, C. He, X. P. Liu, L. Feng, M. H. Lu, Y. F. Chen, *Nat. Mater.* **2016**, 15, 1243.

- [41] X. Liu, S. Xia, E. Jajtić, D. Song, D. Li, L. Tang, D. Leykam, J. Xu, H. Buljan, Z. Chen, *Nat. Commun.* **2020**, *11*, 1586.
- [42] O. Peleg, G. Bartal, B. Freedman, O. Manela, M. Segev, D. N. Christodoulides, *Phys. Rev. Lett.* **2007**, *98*, 103901.
- [43] G. Dávid, J. Cserti, *Phys. Rev. B* **2010**, *81*, 121417(R).
- [44] L. Qifeng, Y. Yonghong, D. Jinming, *Opt. Lett.* **2011**, *36*, 2513.
- [45] J. Cserti, G. Dávid, *Phys. Rev. B* **2006**, *74*, 172305.
- [46] J. Cserti, G. Dávid, *Phys. Rev. B* **2010**, *82*, 201405.
- [47] W. Ye, Y. Liu, J. Liu, S. a. R. Horsley, S. Wen, S. Zhang, *Light: Sci. Appl.* **2019**, *8*, 49.